DOI:10.1190/segam2021-3581137.1

Fault surface objects from fault probability volumes using active contours

Jose Pedro Mora, Heather Bedle, and Kurt. J. Marfurt, School of Geosciences - The University of Oklahoma*

Summary

Seismic surveys provide an invaluable source for understanding depositional histories and structural configurations, important in a range of applications from hydrocarbon accumulations, to geothermal, and carbon sequestration studies. Although manual fault interpretation by a skilled interpreter using knowledge of lithology and structural style usually provides the most accurate fault surfaces, time constraints rarely allow an interpreter to pick every line in a large 3D seismic survey.

For good quality data, horizon mapping is easily accelerated using auto-trackers that follow continuous reflectors, stopping at interpreter-posted discontinuities. Fault digitization is a more complex task, where the interpreter manually picks a grid of fault sticks which are then linked to create a three-dimensional fault mesh. Interpreters often employ coherence images to help them pick a set of fault samples, fault by fault, and line by line, or more commonly, on every n^{th} line. The continuity of coherence images can be enhanced using a variety of nonlinear filters or replaced altogether using convolutional neural networks.

In this study, we use active contours to convert fault probability volumes into a set of fault objects. This study employs a semi-automatic approach that scans high probability fault locations and moves from low to high probability values to fit the fault image's shape. This approach reduces the time to map faults in a seismic section since active contours act as an auto tracker of fault probability or coherence volumes.

Introduction

Fault identification is a manual, time-consuming, and sometimes-uncertain process; many tools are used as an aid to seismic interpreters to map horizons (Pedersen et al., 2002; Goldner et al., 2015). Although many filters can be used to improve the quality of coherence images, converting such images into a fault object is still a difficult task.

Structural features, such as faults or folds, are often easier seen in seismic datasets using attributes related to structural, stratigraphic, and discontinuity properties (Chopra and Marfurt, 2005; Barnes, 2016). In particular, the coherence family of attributes based on crosscorrelation, semblance, eigenstructure analysis, Sobel filters, predictive error filters, and the gradient structure tensor (Bahorich and Farmer, 1995; Marfurt et al., 1998; Gersztenkorn and Marfurt, 1999; Barnes, 2006) provide good fault images. The continuity of coherence images can be enhanced and skeletonized using a variety of nonlinear filters (Pedersen et al., 2002; Barnes, 2006; Aare and Wallet, 2011; Machado et al., 2016; Wu and Hale, 2016; Qi et al., 2019), or replaced altogether using convolutional neural networks (Xiong et al., 2018; Wu et al., 2019; Qi et al., 2020) to create a fault probability volume such as the result shown in Figure 1.

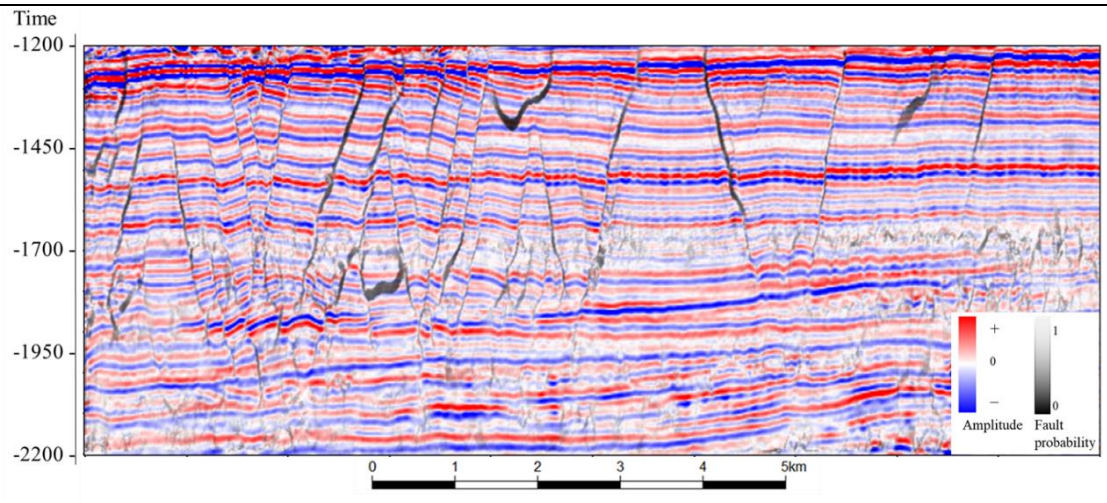

Figure 1: A representative vertical slice through the GSB survey, offshore New Zealand, showing seismic amplitude co-rendered with fault probability using Qi et al.'s (2019) approach. High fault probability values (in black) delineate a suite of normal faults and minor discontinuities associated with mass transport complexes.

Fault surface objects from fault probability volumes using active contours

A common workflow to map faults in seismic datasets uses an amplitude volume co-rendered with a coherence or fault probability volume to provide a means to visualize both values at the same time. Automation in large 3D data sets has been achieved in horizon picking by auto trackers (Dorn, 1998), but manual and semi-automatic digitizing is still a usual way to create fault objects such as fault sticks or three-dimensional meshes. Admasu et al. (2006) and Mora et al. (2020) discuss semi-automatic while Admasu et al. (2006), Cohen et al. (2006) and Wu and Hale (2016) discuss automatic fault object construction.

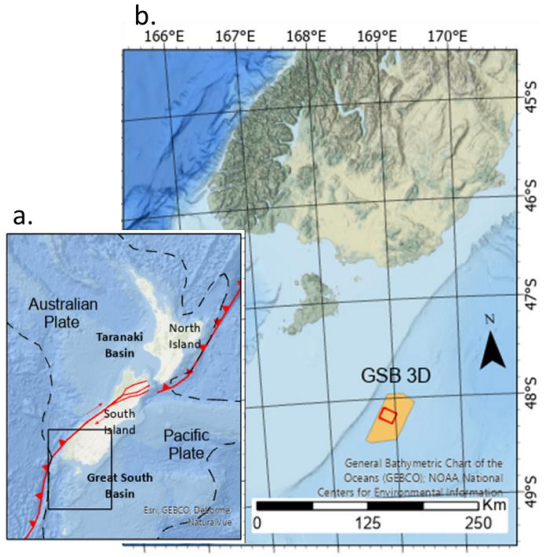

Figure 2. (a) Map of New Zealand showing plate tectonic boundaries and the South Island's strike-slip plate limit. (b) Map of the southern part of the South Island and the GSB seismic volume location.

This study employs a semi-automatic approach to map faults using an active contour algorithm to find high probability values. Active contours scan the initial location of a fault, and the algorithm moves from a point with low to high probability fault values to fit the shape of the fault volume.

Data description

We use a 3D survey in the Great South Basin (GSB) southeast of the South Island, New Zealand (Figure 2). The data were acquired and time-migrated by ExxonMobil and cropped from 1.2 to 2.2 s for this study. We use commercial software for seismic display and conventional fault interpretation, where the faults are exported in a fault stick format.

Active contours

First introduced by (Kass et al. (1988), active contour is a is a computer vision algorithm that attempts to identify shape boundaries in images when the approximated outline is known. This algorithm changes the shape of a polyline and fits it according to the maximum values of an image; it can also create illusory contours fitting values where boundary data are absent (Kass et al., 1988). We follow Admasu et al. (2006) in using this method to map faults.

The active contour model is based on a controlled continuous spline under image forces and external forces. There are three different terms controlling the Snake energy,

$$E^*_{\text{snake}} = \int_0^1 E_{\text{int}}\left(\mathbf{v}(s)\right) + E_{\text{image}}\left(\mathbf{v}(s)\right) + E_{\text{con}}\left(\mathbf{v}(s)\right) ds\,, \quad (1)$$

where E_{int} is the internal energy or line smoothness, E_{image} is the image energy and E_{con} is a constraint term used to guide the contour line towards or away from a particular value.

The internal energy

$$E_{\text{in}} = E_{\text{cont}} + E_{\text{curv}} \quad (2)$$

where the term E_{cont} makes the the contour act as a membrane (line stretch and point distance), and where the term E_{curv} modifies the behavior to act as a thin plate spline (curvature and smoothness) (Kass et al., 1988).

The image energy is defined as

$$E_{\text{image}} = w_{\text{line}} E_{\text{line}} + w_{\text{edge}} E_{\text{edge}} + w_{\text{term}} E_{\text{term}} \quad (3)$$

where w_{line}, w_{edge}, and w_{term} are weights. The first term is the line energy due to the intensity values of the image and will be attracted to high or low values depending on the initial configuration. The second term, or image gradient, acts to attract the contour to large image gradients. The third term is used to find line segment terminations and corners using line curvature.

Methodology

Figure 1 shows a representative vertical slice through the seismic amplitude volume co-rendered with a skeletonized fault-enhanced volume following Qi et al. (2019). We then extract objects from the fault probability volume using active contours. First, we calculate multispectral coherence (Li et

al., 2017); as a second step, we use the weighted energy to seek discontinuities favored by eigenvectors at the reflector locations; in that way, the method reduces stair-step artifacts and enhances fault probabilities (Qi et al., 2019). After we calculate the fault probability, we skeletonize (Qi et al., 2019) to provide input to the active contour extraction method (Figure 3).

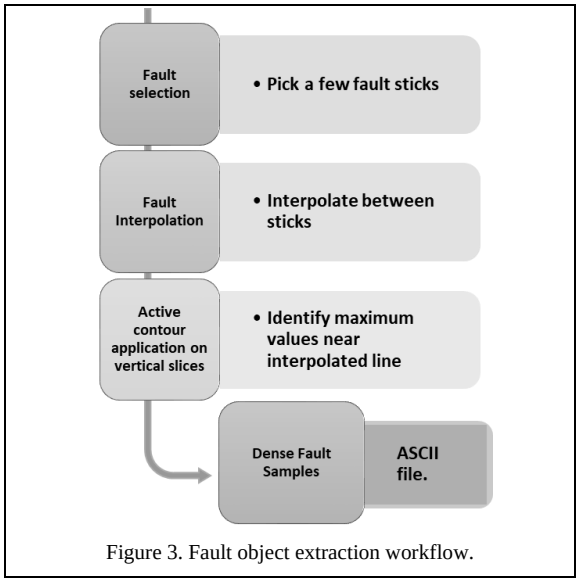

Figure 3. Fault object extraction workflow.

Figure 3 shows the active contour process. We pick fault samples every 10 to 20 lines close to the fault position to define the fault trend. As a second step, we use interpolation methods on the picked samples to create an approximated location in every section near the fault.

The third step is the active contour algorithm calculation, a main fault trend is estimated to define the initial direction of the analysis. The algorithm starts by measuring the distance of the estimated fault, and the algorithm scans the line samples of one fault; then, the algorithm creates a connection between the points to create a spline; the algorithm then starts to find high probability values and smooths the result as shown in Figure 4. Figure 4 shows how the initial fault position (red line) fits the fault position in the section (blue line). The algorithm then moves to a neighboring line and restart the process; at the end of the entire process, a list of adjusted points to fault probability is found.

The final step in Figure 3 is exporting sample values to a stick file format to plot the result in visualization software.

Results

We imported the stick file into commercial software and analyzed it with a seismic volume to see the match between the original data and the extracted surface. We found that active contours lines were fitted to fault probabilities in the lines by scanning image contrast and gradients.

Figure 5 shows the initial interpreted surface, and the extracted result, plenty of samples are created resembling a highly detailed mesh. Visual inspection reveals some non-continuous fault probabilities connected; consequently, the mesh does not have holes or absent samples inside the mesh. Active contours can follow high probability values close to the sample; however, this behavior can drive to automatically attach lines to local maximums not related to the mapped fault, as an example, following channels or to other faults. The previous behavior creates anomalous picks, added to sample creation where there is no data, the interpreter must be aware of these anomalies and remove them manually.

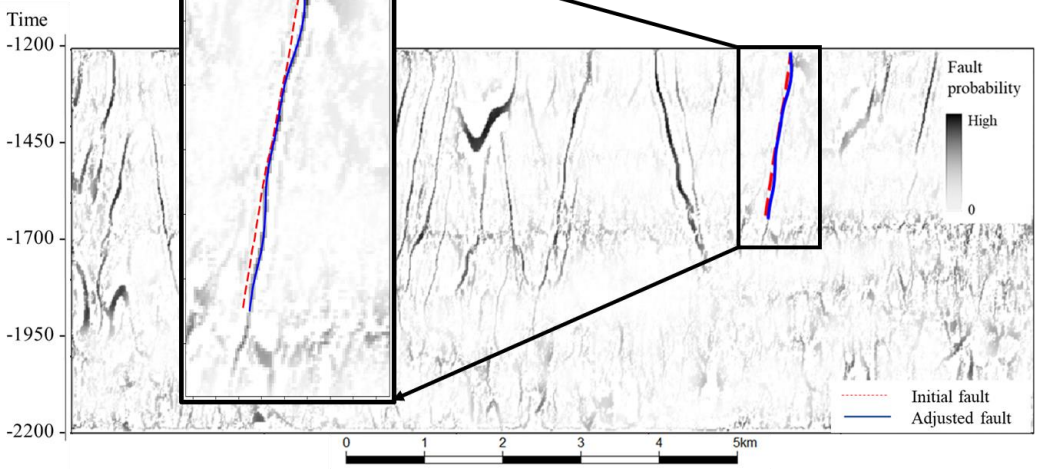

Figure 4. A vertical slice through the fault probability where the initial manual fault pick is defined by the dashed red line. The final active contour mapped fault appears as the continuous blue line. The zoomed inset shows how the initial line moves towards high fault probability values.

The manually fault interpretation generates piecewise linear features that approximate the fault trend. In detail, the fault surfaces are not always straight and planar; the active contours can fit arcuate and listric shapes on vertical slices. The manual picks only need to approximate the fault trend.

In the presence of fault probability noise and artifacts, active contours can get lost; for this reason our recommendation is to use fault enhancement processes (Qi et al., 2019) to smooth and reduce artifacts and undesired features.

Conclusions and future work

Our research proves that it is possible to use active contours to speed up interpretation workflows and optimize time in semi-automatic approaches. The active contour approach shows that it is possible to follow high probability values that resemble a fault in a seismic section, adaptatively changing the line's shape to fit values that match a fault. Seismic attributes sometimes do not show continuous fault probability values due to resolution or quality. However, the active contour can continually draw a fault when voxels do not appear in the processed attribute.

We use this method to create an entire fault object, but active contour has the potential to be used in interactive picking by creating three or four points to guide the spline, and then track high probability values, resembling the fault shape in individual lines acting as an auto tracker.

We think the active contour can use other attributes as additional weights. For example, coherence measures are most accurate at envelope maximum, and we should be able to use this information to better define the fault surface.

In future work, we will compute fault dip, fault azimuth, and fault cylindricity attributes from our more detailed fault surfaces.

Acknowledgments

We want to express thanks to the New Zealand government and the Petroleum and Minerals for the 3D seismic dataset provided, and the Attribute Assisted Seismic Processing and Interpretation (AASPI) consortium for their support. Schlumberger made it possible to use the Petrel at the University of Oklahoma. The first author wishes to thank the Fulbright program and the Saldarriaga-Concha Foundation for their support.

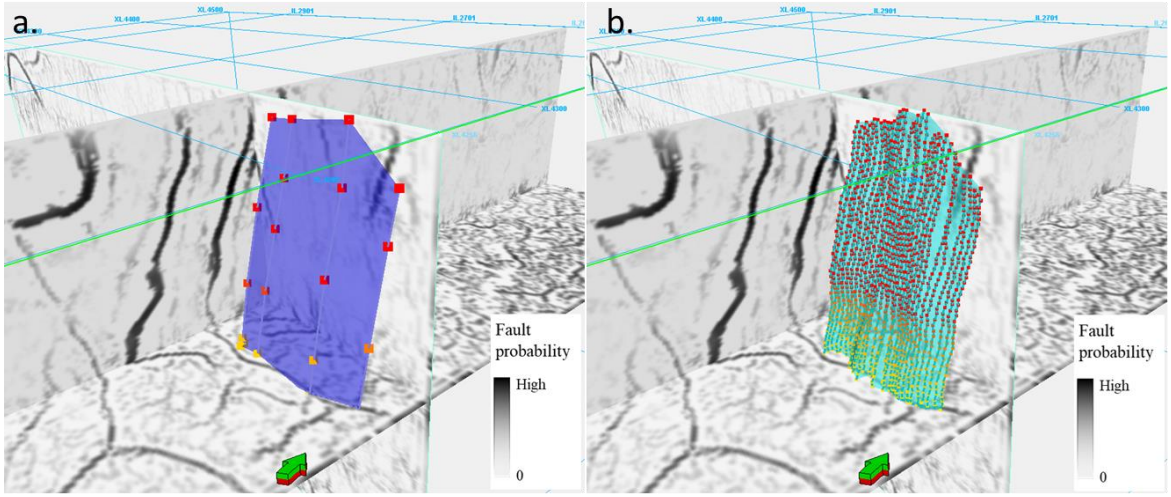

Figure 5. Three slices through the fault probability volume and fault objects. (a) Red dots indicate the initial manual fault picks made on every 10th inline and the resulting spline-interpolated surface. (b) The more detailed fault surface extracted object resulting from active contours, where the detailed fault shape is defined for every inline.

REFERENCES

Aare, V., and B. Wallet, 2011, A robust and compute-efficient variant of the Radon transform: GCSSEPM 31st Annual Bob F. Perkins Research Conference on Seismic Attributes – New Views on Seismic Imaging: Their Use in Exploration and Production, 550–586.

Admasu, F., S. Back, and K. Toennies, 2006, Autotracking of faults on 3D seismic data: Geophysics, **71**, no. 6, A49–A53, doi: https://doi.org/10.1190/1.2358399.

Bahorich, M., and S. Farmer, 1995, 3-D seismic discontinuity for faults and stratigraphic features: The coherence cube: The Leading Edge, **14**, 1053–1058, doi: https://doi.org/10.1190/1.1437077.

Barnes, A. E., 2006, A filter to improve seismic discontinuity data for fault interpretation: Geophysics, **71**, no. 3, P1–P4, doi: https://doi.org/10.1190/1.2195988.

Barnes, A. E., 2016, Handbook of poststack seismic attributes: SEG.

Chopra, S., and K. J. Marfurt, 2005, Seismic attributes – A historical perspective: Geophysics, **70**, no. 5, 3SO–28SO, doi: https://doi.org/10.1190/1.2098670.

Cohen, I., N. Coult, and A. A. Vassiliou, 2006, Detection and extraction of fault surfaces in 3D seismic data: Geophysics, **71**, no. 4, P21–P27, doi: https://doi.org/10.1190/1.2215357.

Dorn, G. A., 1998, Modern 3-D seismic interpretation: The Leading Edge, **17**, 1262–1262, doi: https://doi.org/10.1190/1.1438121.

Gersztenkorn, A., and K. J. Marfurt, 1999, Eigenstructure-based coherence computations as an aid to 3-D structural and stratigraphic mapping: Geophysics, **64**, no. 5, 1468–1479, doi: https://doi.org/10.1190/1.1444651.

Goldner, E. L., C. N. Vasconcelos, P. M. Silva, and M. Gattass, 2015, A shortest path algorithm for 2D seismic horizon tracking: Proceedings of the 30th Annual ACM Symposium on Applied Computing - SAC '15, 80–85, doi: https://doi.org/10.1145/2695664.2695859.

Hale, D., 2013, Methods to compute fault images, extract fault surfaces, and estimate fault throws from 3D seismic images: Geophysics, **78**, no. 2, O33–O43, doi: https://doi.org/10.1190/geo2012-0331.1.

Kass, M., A. Witkin, and D. Terzopoulos, 1988, Snakes: Active contour models: International Journal of Computer Vision, **1**, 321–331, doi: https://doi.org/10.1007/BF00133570.

Li, F., J. Qi, B. Lyu, and K. J. Marfurt, 2017, Multispectral coherence: Interpretation, **6**, no. 1, T61–T69, doi: https://doi.org/10.1190/INT-2017-0112.1.

Machado, G., A. Alali, B. Hutchinson, O. Olorunsola, and K. J. Marfurt, 2016, Display and enhancement of volumetric fault images: Interpretation, **4**, no. 1, SB51–SB61, doi: https://doi.org/10.1190/INT-2015-0104.1.

Marfurt, K. J., R. L. Kirlin, S. L. Farmer, and M. S. Bahorich, 1998, 3-D seismic attributes using a semblance-based coherency algorithm: Geophysics, **63**, no. 4, 1150–1165, doi: https://doi.org/10.1190/1.1444415.

Mora, J. P., H. Bedle, and K. J. Marfurt, 2020, Constructing fault-surface objects from fault-sensitive attributes: 90th Annual International Meeting, SEG, Expanded Abstracts, 1160–1164, doi: https://doi.org/10.1190/segam2020-3425159.1.

Pedersen, S. I., T. Randen, L. Sonneland, and O. Steen, 2002, Automatic 3D fault interpretation by artificial ants: 64th Annual International Conference and Exhibition, EAGE, Extended Abstracts, cp-5, doi: https://doi.org/10.3997/2214-4609-pdb.5.G037.

Qi, J., B. Lyu, X. Wu, and K. Marfurt, 2020, Comparing convolutional neural networking and image processing seismic fault detection methods: 90th Annual International Meeting, SEG, Expanded Abstracts, 1111–1115, doi: https://doi.org/10.1190/segam2020-3428171.1.

Qi, J., B. Lyu, A. Al Ali, G. Machado, Y. Hu, and K. Marfurt, 2019, Image processing of seismic attributes for automatic fault extraction: Geophysics, **84**, no. 1, O25–O37, doi: https://doi.org/10.1190/geo2018-0369.1.

Wu, X., and D. Hale, 2016, Automatically interpreting all faults, unconformities, and horizons from 3D seismic images: Interpretation, **4**, no. 2, T227–T237, doi: https://doi.org/10.1190/INT-2015-0160.1.

Wu, X., L. Liang, Y. Shi, and S. Fomel, 2019, FaultSeg3D: Using synthetic data sets to train an end-to-end convolutional neural network for 3D seismic fault segmentation: Geophysics, **84**, no. 3, IM35–IM45, doi: https://doi.org/10.1190/geo2018-0646.1.

Xiong, W., X. Ji, Y. Ma, Y. Wang, N. M. AlBinHassan, M. N. Ali, and Y. Luo, 2018, Seismic fault detection with convolutional neural network: Geophysics, **83**, no. 5, O97–O103, doi: https://doi.org/10.1190/geo2017-0666.1.